Building and Environment 184 (2020) 107248

Contents lists available at ScienceDirect

Building and Environment

journal homepage: http://www.elsevier.com/locate/buildenv

Simulation of spectators' aerodynamic drag using porous models approximation

Ahmed Osama Mahgoub [a,*], Saud Ghani [a], Mohammed M. Rashwan [a], Salman M. Ismail [a], Esmail A. ElBialy [b]

[a] Department of Mechanical and Industrial Engineering, Qatar University, P.O. Box 2713, Doha, Qatar
[b] Faculty of Engineering, Cairo University, Postal Code, 12613, Giza, Egypt

ARTICLE INFO

Keywords:
Aerodynamics
CFD
Drag force
Porous media model approximation
Stadiums
Thermal comfort

ABSTRACT

Evaluation of the thermal comfort is essential for complex ventilation systems design. Assessment of thermal indices requires representative velocity and pressure fields' values. When simulating the air flow in large facilities such as stadium, the effect of crowds' geometrical features needs to be captured. Using porous models approximations to simulate the aerodynamic effect of detailed spectators' geometry reduces the required mesh size and associated processing time. This paper investigates the use of different porous media models approximations for capturing the effect of large crowds inside complex building systems, such as stadiums. Their efficiency of capturing the effect of spectators on the air flow were compared to the simulation of the exact spectators' geometry. The exact spectators' geometrical model was of a stadium tiers section with 28 spectators. Using a wind tunnel, the exact spectator's model results were validated against a 1:10 scaled physical model. The experiments included PIV and hot-wire velocity measurements. The results of the pressure drop were used to obtain the coefficients needed to utilize the porous models. Compared to the exact spectators' case, the three-dimensional porous volume model approximation yielded an average absolute error of 24.5% in velocity, while the two-dimensional porous jump model yielded results with an average error of 1.5%. In comparison to the exact model cooling load, the results yielded a difference of 6% for the 2D porous jump and 6.5% for the 3D porous volume. Nevertheless, both models yielded more representative results than the case of simulation of empty bleachers.

1. Introduction

Providing acceptable thermal environment for large crowds attending events in large facilities such as stadiums is a challenge for designers. Heating, ventilation and air-conditioning (HVAC) systems allow the climate control of such environments. However, experiments or representative numerical simulations are needed for reliable HVAC systems design. At the design phase, it is difficult to experimentally evaluate the HVAC system performance. Therefore, computational fluid dynamics (CFD) is used to ensure providing the spectators with the required thermal microclimate by supplying ventilation. Utilization of CFD in various applications of different flow regimes offered a credible alternative to experimental testing [1] providing reliable numerical tools [2]. For stadiums, an adequate 3D model should be able to replicate the exact geometrical and physical details of the stadium's tiers and the seated spectators. The bluff bodies of spectators present an aerodynamic drag resistance to the movement of the conditioned air trickling down the tiers.

Inside stadiums, accurate assessment of the spectators' and players' thermal comfort is of utmost importance. CFD case studies aid in the designing of HVAC systems for such outdoor environments. However, it is not feasible to describe each individual spectator geometry at a detailed level. HVAC systems' performance can be verified by evaluating various microclimate thermal comfort indices. Several thermal indices are currently used for specific environments [3]. Thermal indices are functions of the velocity field [4]. Current numerical simulations model the stadiums' geometries with empty tiers. This leads to an anomaly in the predicted velocity values, which in turn leads to an error in predicting HVAC system design specifications and performance.

1.1. Numerical simulation of complex ventilation systems

Stadiums are considered as semi-opened areas and are affected by

* Corresponding author.
E-mail address: ahmed.mahgoub@qu.edu.qa (A.O. Mahgoub).

https://doi.org/10.1016/j.buildenv.2020.107248
Received 5 August 2020; Received in revised form 26 August 2020; Accepted 29 August 2020
Available online 1 September 2020

Nomenclature

AHU	Air handling unit
ASHRAE	American society of heating, ventilation and air conditioning engineers
CFD	Computational fluid dynamics
DV	Displacement ventilation
HVAC	Heating, ventilation and air-conditioning
MCV	Mean comfort vote
PIV	Particle image velocimetry
PMV	Predicted mean vote
PPD	Predicted percentage of dissatisfied
RANS	Reynolds-averaged Navier-Stokes
SET	Standard effective temperature
UTCI	Universal thermal climate index
WBGT	Wet-bulb globe-temperature
C_0, C_1	Power law coefficients
C_2	Inertial resistance coefficient (m^{-1})
C_p	Specific heat of air (kJ/kgK)
dw	Humidity ratio difference (kg/kg)
FoP	Field of play
h_{total}	Total cooling load (kW)
$h_{sensible}$	Sensible heat (kW)
h_{latent}	Latent heat (kW)
h_{we}	Latent hear of evaporization water (kJ/kg)
q	Volumetric flow rate (m^3s^{-1})
R2	Coefficient of determination
RH	Relative humidity (%)
T_{air}	Air temperature (°C)
dT_{air}	Temperature difference (°C)
u	Velocity of air (m s^{-1})
$x, y z$	Cartesian coordinates
Δn	Thickness of porous medium (m)
k	Turbulent kinetic energy (m^2 s^{-2})
ε	Turbulent dissipation rate (m^2 s^{-3})
p	Pressure (Pa)
Δp	Pressure drop (Pa)
S_i	Sink term for the porous media model
μ	Kinematic viscosity of air (m^2 s^{-1})
ρ	Air density (kg m^{-3})
$1/\alpha$	Viscous resistance coefficient (m^{-2})

wind, weather conditions and the surrounding urban planning. The shape of a stadium's roof can additionally affect the wind load [5]. The stadiums' internal and external aerodynamics have been investigated using CFD. However, the stadium's complex geometry present a challenge when performing numerical CFD simulations. Previous CFD studies highlighted that the stadium air quality is affected by the stadium's design [6,7] and by the incident wind direction [8–11]. Chen and Li [12] investigated the optimal inlet wind angles for different stadia and concluded that they range from 75° to 90° [12]. Blocken and Persoon investigated the effect of Amsterdam Arena stadium on the pedestrian wind comfort using the Dutch wind nuisance standards (NEN 8100: 2006, NPR 6097: 2006). The authors concluded that CFD overestimated human discomfort up to 25% [13]. Wind driven rain was simulated for AZ Alkmaar stadium in Netherlands. The study highlighted the role of the structure's geometry, in particular the roof slope, on the formation of wet areas caused by wind-driven rain. CFD studies were used to propose design guidelines for structural improvements [14–16]. CFD was also used to assess the efficiency of stadium's ventilations systems. In Japan [17], simulated the Tokyo Olympic Stadium applying CFD analysis and GIS approach, to an integrated Airflow Analyst model. The results were validated with an experimentally reproduction of the stadium examined in a wind tunnel. The study showed good agreement, with respect to the conditions of the wind flow ventilation from the sky. In 2020, Kim and Jong combined microclimate and CFD models for evaluating the flow field around a stadium. It was found that this combined simulation method was able to accurately predict the detailed air flow. The microclimate model was used to obtain the wind direction and speed based on the configuration of the district where the stadium building site is proposed [18].

For turbulence modeling, Reynolds-Averaged Navier Stokes (RANS) and large-eddy simulations (LES) models were used. Zheng et al. [19] assessed the performance of RANS and LES for predicting the pressure field for buildings with balconies. The presence of balconies in buildings led to turbulent regions characterized by separation and recirculation areas. The results showed that for wind directions perpendicular to the façade, both RANS and LES predicted the pressure coefficient accurately [19].

1.2. CFD for thermal comfort prediction

Understanding the thermal and dynamic influence of the wind on the human body thermal sensation is essential for designing and assessing comfortable and safe outdoor environments [20]. The global assessment of the thermal comfort of players and spectators inside stadiums is vital for ventilation systems design and control. Mahgoub et al. [21] proposed a methodology for the global thermal comfort evaluation of the wet-bulb globe-temperature (WBGT) and the standard effective temperature (SET) for spectators. The study was able to generate results with an error less than 2% compared to point-wise evaluation [21]. In regions with hot climates, the grass that covers the large area of the field of play (FoP) changes the temperature field inside the stadium, which in turn affects thermal comfort of players [22].

Currently, CFD is extensively used to assess the human thermal comfort in the indoor and outdoor built environments. Earlier studies focused on indoor environments [23]. Catalina et al. [24], tested the efficiency of a radiant cooling ceiling, using predicted mean vote (PMV) plots, arguing that thermal comfort was evenly distributed in an examined room [24]. For offices, PMV and the predicted percentage of dissatisfied (PPD) were accurately predicted using CFD [25]. For a wider range of facilities and premises in Hong Kong, such as offices, classrooms, retail shops and industrial workshops, CFD was used to assess mixing and displacement ventilation (DV) thermal indices, promoting the latter for higher indoor human thermal comfort [26].

With regard to outdoor environments, thermal comfort is of interest in places where large events are held, such as stadiums and amphitheaters. Ghani et al. [3]validated five thermal comfort indices, namely mean comfort vote (MCV), WBGT, Discomfort Index, Cooling Power index and Humidex simulated values against thermal sensation surveys [3]. CFD results overestimated the value of the first three indices while underestimating the latter two. In the tropics, CFD simulated temperature, air flow rate and relative humidity in a lecture theatre, overestimating air velocity and air temperature. Occupants were modeled using simplified box shapes [27]. Stamou et al. [28]used CFD to evaluate thermal comfort in an Amphitheatre of the Athens Olympic games 2004. Their simulation used CFD predicted velocities and temperatures to evaluate the PMV and the PPD. The results showed satisfactory thermal conditions for inlet air of 16.5°C [28]. For stadiums used for Athens 2004 Olympic Games, CFD simulated PMV and PPD values that were found to be satisfactory to more than 93% of the spectactors [29,30]. In the study, spectators were modeled based on the surface area and the heat generated by each individual.

1.3. Use of porous media models in buildings' simulations

For numerical simulation of the air flow in buildings with complex geometrical features, porous media models can be used. The porous media models represent the macroscopic flow effects of a porous structure without modeling the microscopic flow details [31]. Several investigations were carried out using the porous models to examine the fluid flow regimes and penetration in porous media. The 3D porous volume model was used to examine ventilation of dairy cow buildings in Denmark [32], and to characterize climatic conditions in a greenhouse considering ripe tomatoes as porous medium [33–35]. In Switzerland, the 3D porous volume model was utilized to investigate the effect of local wind flow profile on non-uniform drying of the urban surfaces [36]. The authors stated that the complex spatial and temporal interplay among the climatic inputs made the modeling process more complicated. Ooi et al. [37] used a 3D porous volume model to simulate the louvers on buildings' facades. They were able to predict velocities using the porous media, and the error ranged from 10% for simple models to 38% for complex designs [37]. The 2D porous jump model is extensively used in CFD for filtration, porous substrates, packed bed, and macro-porous material investigations [38–43]. The applicability of porous media models is not limited to buildings with complex geometries, but can also include simulations of vegetation barriers [44].

1.4. Motivation and objectives

In order to perform representative CFD simulations for human thermal comfort investigations, the effect of the presence of the spectators must be included. Human spectators act as bluff bodies when they are immersed in air. When bluff bodies are placed in air flow streams, they alter the velocity field, generating separated flow over a substantial proportion of their surface [45]. The aerodynamic performance of shapes immersed in a flow is determined by their drag coefficient and the pressure distribution [46]. The main challenge for predicting drag force of bluff bodies exposed to air flows is that the calculated drag coefficient value is always lower than the measured value [47].

Computationally, it is not practical nor feasible to simulate the detailed geometrical features of every seated spectator in the stadium. This research assesses the feasibility of using two porous models to capture the drag effect presented by seated spectators in an air-conditioned stadium to the prevailing air flow. The seated spectators are considered as bluff bodies or obstacles generating a resistance to the flow of conditioned air released from the air supply nozzles or diffusers. The numerical model flow field results of a partial section of the stadium with detailed geometry of 28 seated spectators are experimentally validated against wind tunnel measurements of velocity and pressure values. Hence, the results of the porous models with adjusted coefficients are compared with their counterpart model with the exact spectators' geometry. The velocity fields obtained when using empty bleachers and the porous models are compared to the case of detailed spectators' geometry. Finally, two thermal comfort indices (SET and UTCI) are evaluated and the cooling load is calculated for each case to demonstrate the effect of the developed velocity fields on their values and to assess the performance of the different models.

This work provides engineers, designers and practitioners with a tool for determining the coefficients needed when using the porous media models to simulate the effect of spectators when performing CFD simulations for large crowds without the need to model the detailed geometry of the spectators.

This paper is structured as follows: In section 2, the methodology used for performing experiments and numerical simulations is discussed. Hence, section 3 provides the results of the numerical simulations for the different cases and models, the validation against experimental results, and the effect of the velocity field on thermal comfort indicators. Finally, in section 4 conclusions are drawn and recommendations for future work are given.

2. Methods

In this section the methodology used for experimental testing and CFD simulations is discussed. Fig. 1 presents the methodology roadmap adopted to assess the utilization of the porous models. The flow diagram is branched into a numerical study and an experimental study and validation of the flow field velocity and pressure values.

2.1. Geometrical configuration

The study was carried for Al-Thumama international stadium, Doha, Qatar, 25°14′06.5″N 51°31′55.3″E. The stadium is designed for a capacity of around 40,000 spectators. The stadium, of 240 m diameter and 43 m outside clear height, is oriented North-South as specified by FIFA [48]. Fig. 2 shows the geometry of the stadium under investigation. The stadium bowl air conditioning system utilizes various air handling units (AHU), under seat diffusers and nozzles to deliver the conditioned air to the stadium tiers and FoP.

A detailed 3D geometrical model of a partial section of the stadium tiers and 28 spectators was utilized to simulate the drag effect of seated spectators on the air flow. Each spectator has a height of 1.35 m and a width of 0.4 m. Fig. 3 shows the model geometry of a 5.6 m in width, 12 m in height and 12 m in depth.

2.2. Experimental tests

The experiments were performed at Qatar University's low speed closed circuit wind tunnel with a test section of 2 × 2 m. A 1:10 scaled down plexiglass model representing the stadium partial tiers with 28 3D printed seated spectators was manufactured to be used for testing. The model had 28 seated spectators, sitting across seven rows of the stadium section. The acquired velocity and pressure values were used for the validation. Velocity measurements were performed using both hotwire anemometry and particle image velocimetry (PIV).

Air velocity measurements were recorded using a Testo 435 hot wire anemometer. The selected probe has an outer diameter of 7.5 mm, to minimize the effect of the presence of the probe geometry on the prevailing air flow. The probe has a velocity measuring range of 0–20 m/s with a resolution of 0.01 m/s. A Fluke 922 air flow micro-manometer was used to measure the developed air dynamic pressure. The device has a range of ±4000 Pa, resolution of 1 Pa and an accuracy of ±1% Pa.

2.2.1. Pressure and hotwire velocity measurement

For the CFD model validation, the flow field pressure and velocity values were measured for the flow past the 3D printed model. Fig. 4 shows the model while placed inside the wind tunnel, where air is blowing parallel to the bleachers. Air velocity and pressure values were measured for five different free stream velocities of 0.3 m/s, 0.5 m/s, 0,7 m/s, 0.9 m/s, and 1.1 m/s. In order to calculate the overall pressure drop across the spectators body, measurements of pressure values were taken at the two vertical planes upstream (at 18 points) and downstream (at 27 points) the seated spectators body. Moreover, both velocity and pressure values were measured at eight points along a line cutting through the seven rows of seated spectators.

2.2.2. Velocity measurement using particle image velocimetry (PIV)

Particle image velocimetry (PIV) is an experimental tool to non-intrusively obtain the velocity of a whole flow field. PIV is based on detecting the light scattered from tracer particles injected in a flow. It uses two consecutive images of a flow field seeded by particles. By cross correlation of the two images, the displacement of each group of particles can be estimated, and from the knowledge of the time between the frames, a corresponding velocity is obtained [49,50]. The particles are illuminated at two different time instants by means of a double pulsed laser sheet. For air flow seeding, smoke particles of mean diameter of $1\mu m$ were used. The particles were generated using a fog generation

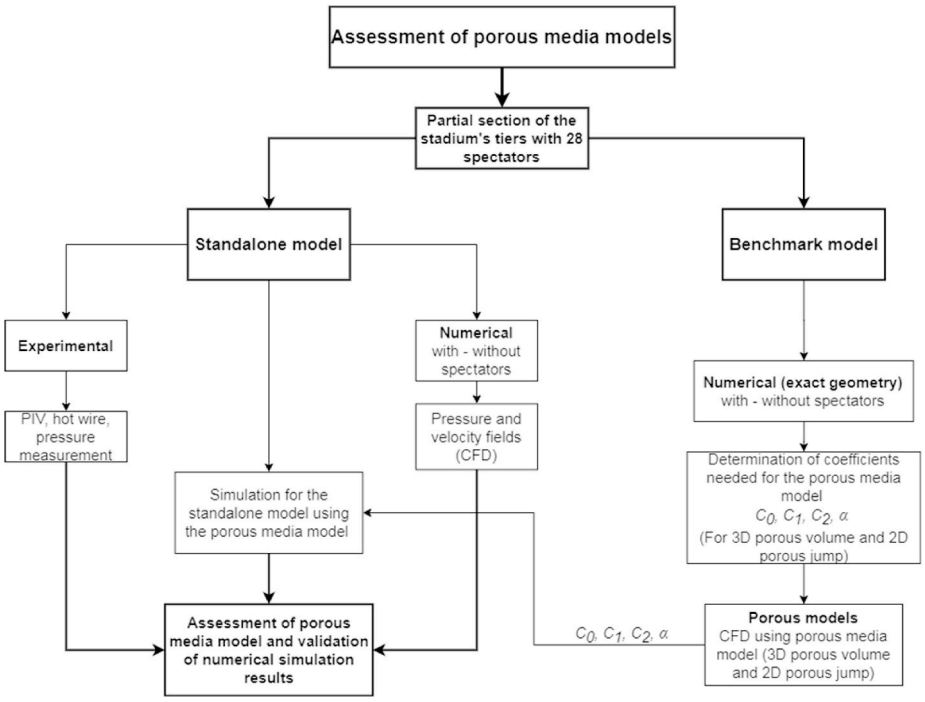

Fig. 1. Flow diagram of the porous models assessment procedure.

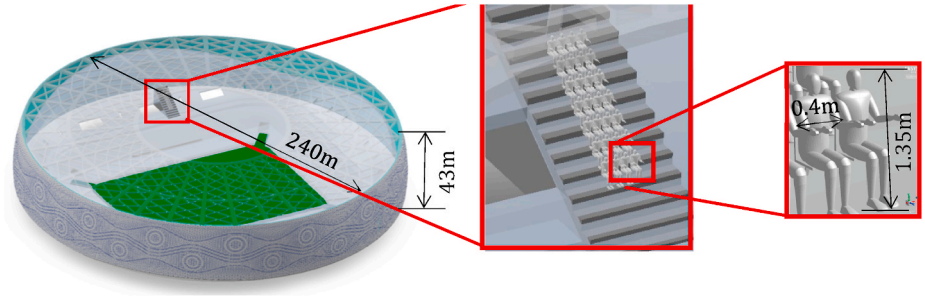

Fig. 2. Location of area under investigation in Al-Thumama stadium.

machine (Safex F2010). The laser used was Dantec Dynamics DualPower 200-15, which is a twin cavity Nd:YAG laser of wavelength 532 nm and a pulse duration of 4 ns. Maximum laser power is 1200 mJ. A FlowSense EO 4 M CCD camera from Dantec Dynamics, with a resolution of 2048× 2048 pixels, was used. For processing of the acquired images and results, DynamicStudio software was used [51]. A computer is used for controlling the system and processing the PIV data. A synchronization unit is connected to the computer to allow the control of the data acquisition process. Fig. 5 shows a schematic illustrating the experiment setup and PIV system components.

In order to obtain the velocity field, a set of 50 double frame images were acquired at a triggering frequency of 7.4 Hz, which spans a period of 6.75 s. The time between the light pulses, which is also the time between the two frames of a double frame image, is 500 μsec. Each double frame image, gives a velocity field, and therefore 50 velocity fields were obtained, and were averaged to obtain the final result. The interrogation window size was set to 32 × 32 pixels with 50% overlap in both the horizontal and vertical directions, which resulted in a 127× 127 vectors map. The PIV measurements were performed on the first column of spectators on the right of Fig. 4. The spectators were sprayed with black paint to minimize laser sheet reflections.

2.3. Numerical simulation

In this subsection, the details for the numerical simulations performed are given. ANSYS Fluent version 18.1 commercial software is used to perform the numerical simulations.

The geometrical model is built to accurately mimic the detailed features of a partial section of the stadium's tiers' structure and 28 seated spectators. Mainly, two computational domains were developed for simulations. The first model, referred to as the "benchmark model", is made in such a way to represent a portion of the stadium, with the sides defined as symmetry planes (to simulate the effect of the other tiers). The second model, referred to as the "standalone model", is exactly similar to the earlier model, with the only difference being that it is a placed in the middle of a virtual wind tunnel computational domain. The standalone model is mainly used for validation against experimental wind tunnel results. Mimicking the exact conditions in the whole stadium requires producing models to represent the connectivity with the other tiers (represented by the symmetry boundary condition in CFD), which is not feasible. For the benchmark and the standalone models, 3D porous volume and 2D porous jump models were assessed.

2.3.1. Mathematical modelling

The numerical solver solves the steady incompressible Navier-Stokes

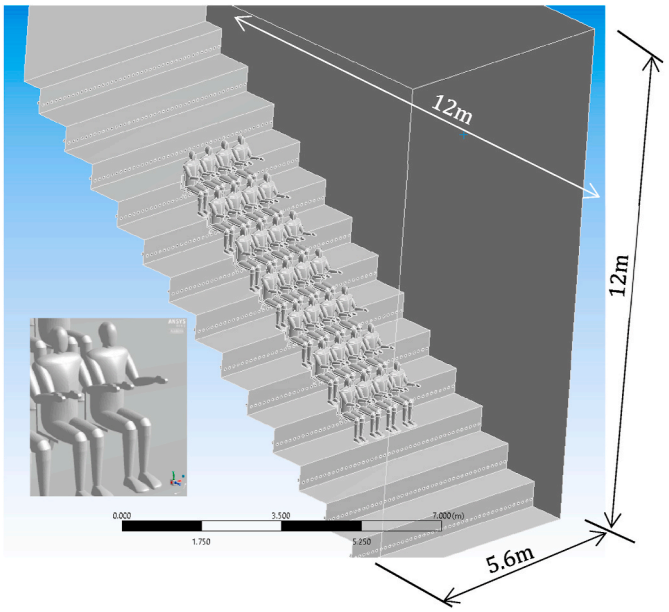

Fig. 3. 3D modeled sample of seated spectators.

equations coupled with the porous media model as follows

$$\frac{\partial u_i}{\partial x_i} = 0, \tag{1-a}$$

$$u_j \frac{\partial u_i}{\partial x_j} = \nu \frac{\partial^2 u_j}{\partial x_j^2} - \frac{1}{\rho}\frac{\partial p}{\partial x_i} - S_i \tag{1-b}$$

where u_i is the component of the velocity field in the i-th direction (m/s), ν is the kinematic viscosity coefficient (m^2/s), p is the pressure field (Pa), ρ is air density (kg/m^3), and S_i is the sink term due to the effect of the porous media model in the i-th direction. For a homogeneous (isotropic) porous medium, S_i is the same in all directions $i = 1, 2, 3$.

In the momentum equation (equation (1-b)), the sink term due to the porous media model is defined as follows:

$$S_i = -\left(\frac{\mu}{\alpha}u_i + C_2\frac{1}{2}\rho|u|u_i\right) \tag{2}$$

where $1/\alpha$ is the viscous resistance coefficient, and C_2 is the inertial resistance coefficient.

Equations (3)–(7) are in accordance with FLUENT user inputs for porous media of a thickness of Δn [52]. ANSYS FLUENT allows the source term to be modeled as a power law of the velocity magnitude:

$$S_i = -C_0|u|^{C_1} \tag{3}$$

where, C_0 and C_1 are user-defined empirical coefficients.

By examining equation (1-b), it can be noticed that the sink term of the porous media model is analogous to the pressure gradient,

$$\nabla p = S_i \tag{4}$$

The pressure drop across the porous medium can be obtained as follows:

$$\Delta p = -S_i\,\Delta n \tag{5}$$

Where, S_i is the momentum source term, and Δn is the porous media thickness. Substituting equation (3) for S_i in equation (5), yields the following:

$$\Delta P = \Delta n\, C_0|u|^{C_1} \tag{6}$$

Equation (6) allows obtaining the coefficients C_0 and C_1 from the knowledge of the pressure drop. The pressure drop across a porous region can also be evaluated by a second order polynomial, as follows:

$$\Delta p = A\,u^2 + B\,u \tag{7}$$

Where, Δp is the pressure drop and u is the velocity. Combining equations (2) and (5), and comparing them to equation (7), allows obtaining the coefficients C_2 and $1/\alpha$ needed for the porous media model from the knowledge of the pressure drop.

The standard k-ε model with enhanced wall treatment is used for turbulence modeling. It was first developed by Ref. [53]. The model presents a good compromise between realistic description of turbulence and computational efficiency [54], and was used for comparative parametric studies. Linden [55] examined the reliability of the standard k-ε for the prediction of natural ventilation [55]. The model performance was also evaluated for real size systems [55–58]. Further guidelines for accurate CFD simulations for urban physics were provided by Ref. [59].

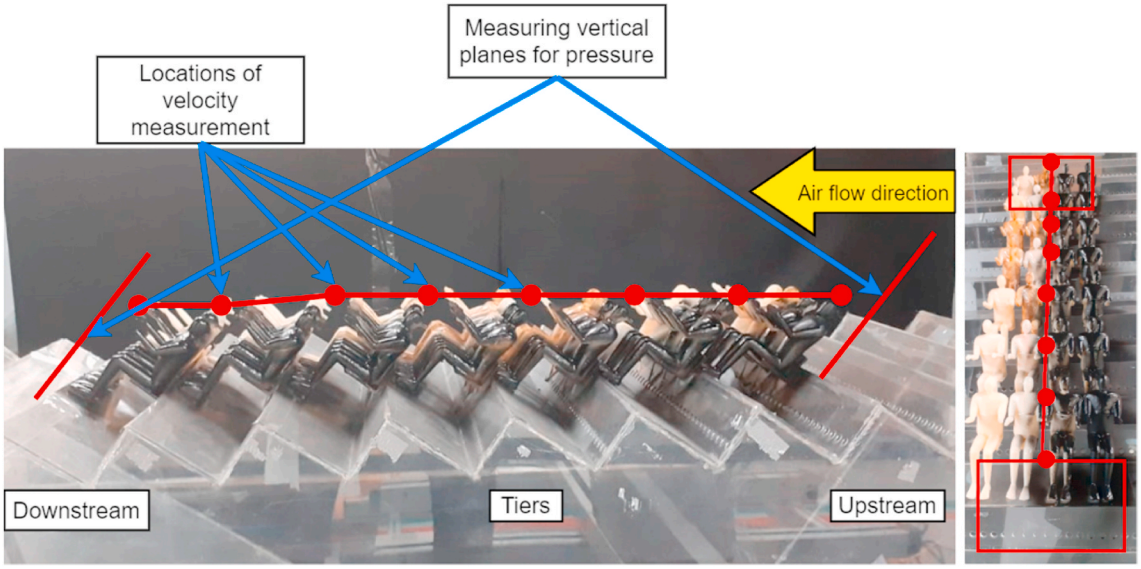

Fig. 4. 3D printed model of 28 spectators placed in the wind tunnel.

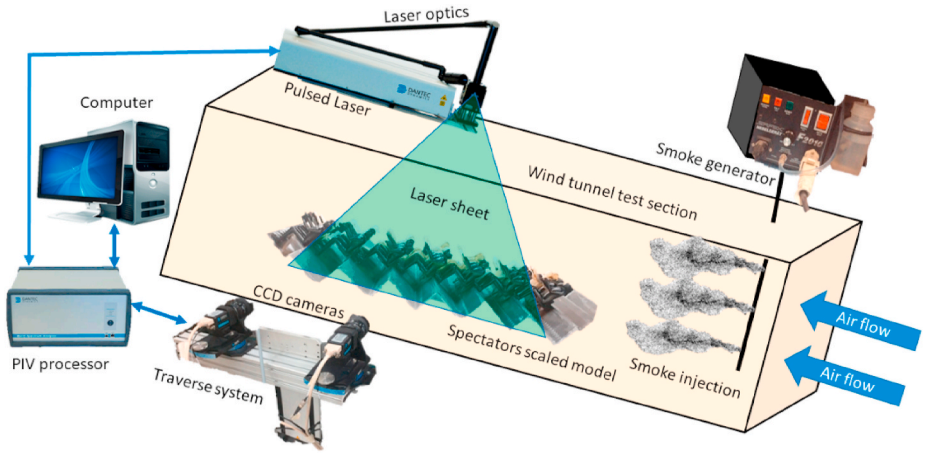

Fig. 5. Schematic of the PIV experiment setup and system devices.

2.3.2. Computational domain for the benchmark model

Fig. 6 shows the computational models developed for the benchmark model. The size of the computational domain was as shown in Fig. 3, and the sides were defined as symmetry planes. To capture the maximum aerodynamic effect of the bulk of the spectators' bodies, the inlet to the domain was considered to be upstream the spectators. The grid for the stadium section with 28 detailed spectators had about 12,000,000 tetrahedral cells. While keeping the same maximum cell size, a second model of around 900,000 tetrahedral cells was created with the spectators' region represented by a three-dimensional porous volume. Hence, a third model of about 900,000 tetrahedral cells was created with a two-dimensional porous jump representing each spectators' row. The grid sizes were selected according to a grid independence study, to ensure that the numerical results are independent of the model mesh size or type. Four different models of mesh size 7, 15, 20 and 28 million cells were used to assess the solution's grid independence. For the model with detailed spectators, the grid with 20 million cells was selected for further simulations.

2.3.3. Computational domain for the standalone model

A standalone model in a virtual wind tunnel domain was developed for validation against the 1:10 scaled model. Fig. 7 presents the computational domain and the surface grid used for the standalone model. The computational domain shown had a length equal to 18 times the model width, a width that was six times the model width, and its height was six times the model width. Two models were simulated, and hence two grids with different sizes were generated. For the model with the detailed spectators, the total number of grid cells exceeded 25 million. For the model without spectators, a grid of 1.5 million cells was used. As the computational domain in this model represents the wind tunnel working section, the total number of grid cells was larger than the ones used for the benchmark model. Two other standalone models were developed to test the usage of the porous media model, after obtaining the required porous media model coefficients.

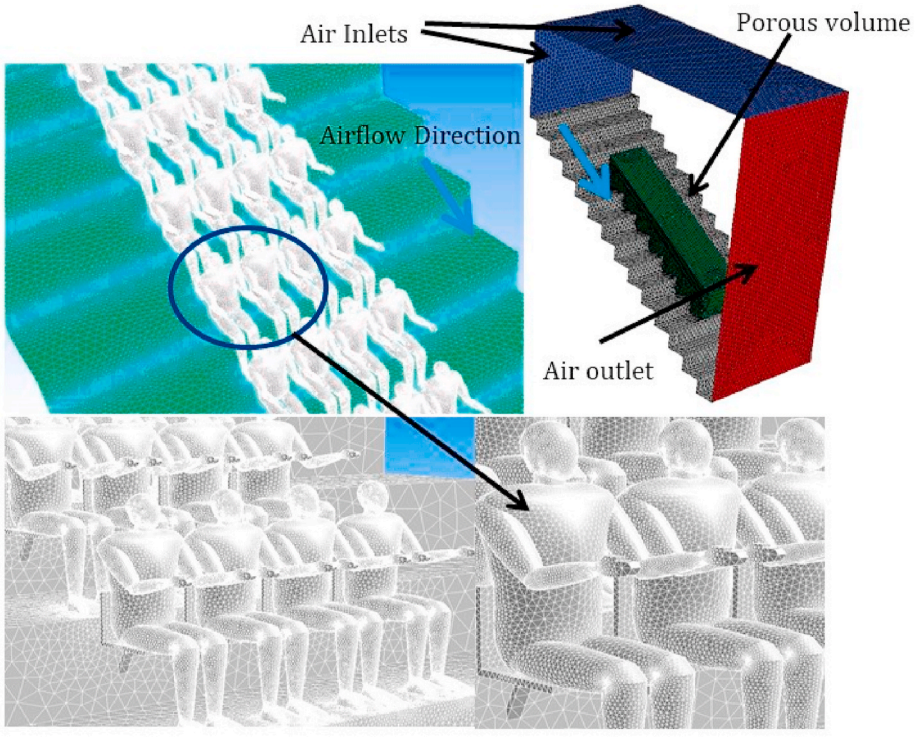

Fig. 6. Computational domain and surface mesh for the benchmark model.

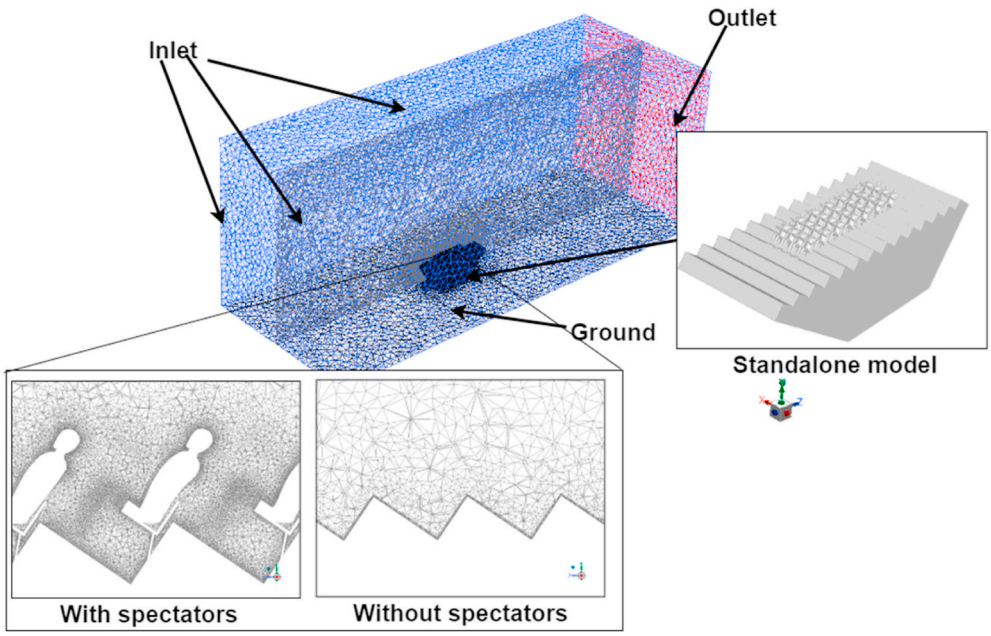

Fig. 7. Computational domain for the standalone validation model and surface grid at different locations.

2.3.4. Boundary conditions

Since the flow field is solved in an iterative method, initial values are needed. Moreover, the values of flow variables (or their gradients) at the model boundaries need to be specified. The simulation was initialized with a zero velocity flow and turbulence fields. Other specific boundary conditions used are given in Table 1. The first part of this study is concerned with the spectators' effect on the velocity field. Therefore, thermal effects are not considered. However, later, the energy and the species transport models were used to evaluate the thermal comfort indices and calculate the cooling load for the various cases.

2.4. Calculation of thermal comfort indices and cooling load

Thermal comfort for spectators inside stadiums can be assessed using the standard effective temperature index (SET). SET was proposed by the American society of heating, ventilation and air-conditioning engineers (ASHRAE) and it is defined as: "the dry bulb temperature of a hypothetical isothermal environment of 50% relative humidity in which a subject, while wearing clothing standardized for activity concerned, would have the same heat stress and thermo-regulatory strain as in the actual test environment" [60]. The SET is a function of air temperature, relative humidity, velocity, pressure, clothing ratio, and metabolic rate. The details for the methodology used for evaluating the SET is provided by ASHRAE [60].

Table 1
Boundary conditions for the benchmark and standalone models.

Boundary	Type	Standalone validation model	Benchmark model
Air inlets	Velocity inlet	Free stream velocity of 3 m/s. Turbulent intensity was set to 5% and viscosity ratio to 10.	Simulations were performed using velocity values ranging from 0.1 to 3 m/s. The velocity inlet direction vector was equal to the slope of the stadium tiers (approximately 31.5°). Turbulent intensity was set to 5% and viscosity ratio to 10.
Air outlet	Pressure outlet	Gauge pressure of 0 Pa. Turbulence intensity 5% and viscosity ratio of 10.	
Spectators, tiers, and ground.	Walls	stationary, no-slip, smooth walls	
Domain sides	Symmetry	None	Symmetry boundary condition was applied to the domain sides.

Another thermal index assessed in this study is the universal thermal climate index (UTCI), which can be used for both indoor and outdoor environments [61]. UTCI was developed in the beginning of 2000s by a number of scientists and experts [62]. Similarly to the SET, when evaluating UTCI, the air velocity, temperature, and relative humidity are taken into account [63]. In this study, both the SET and the UTCI are evaluated for the assessment of the porous models. Misrepresentation of air velocity values leads to errors in thermal comfort assessment. When simulating air flow inside a stadium without spectators, the velocity field will not be representative of the real case with spectators, and prediction of SET and UTCI values will yield anomalies.

To evaluate the energy required for an HVAC system operation, the cooling load needs to be calculated. The total cooling load can be calculated as follows:

$$h_{total} = h_{sensible} + h_{latent} \tag{8}$$

where h_{total} is the total cooling load (kW), $h_{sensible}$ is the sensible heat (kW), and h_{latent} is the latent heat (kW). The sensible and latent heat terms can be calculated as follows:

$$h_{sensible} = \rho q C_p dT_{air} \tag{9}$$

$$h_{latent} = \rho q h_{we} dw \tag{10}$$

where ρ is the air density (kg/m^3), q is the volumetric flow rate, C_p is the specific heat for air (kJ/kgK), h_{we} is the latent heat of water evaporization (kJ/kg), dT_{air} is the air temperature difference between the conditioned air and the ambient temperature (K), and dw is the humidity ratio difference between conditioned air and outer region (kg/kg). The specific heat for air is taken as 1.006 kJ/kg.K and the latent heat of evaporization water is 2454 kJ/kg.

3. Results and discussion

In this section, the results obtained from the experimental testing and CFD simulations are presented. The numerical simulation results for the standalone model were validated against the experimental results acquired from the wind tunnel.

3.1. Validation of the numerical model

The numerical model flow field results of velocity and pressure were validated against wind tunnel measured data. Air velocity and pressure values were measured upstream and downstream the group of seated spectators and along a line cutting through the seven rows of seated spectators. Air velocity and pressure were recorded at five different air blowing velocities of 0.3, 0.5, 0.7, 0.9 and 1.1 m/s. These velocities were used for the full scale geometry (CFD simulations). To satisfy dynamic similarity requirements, the velocities tested for the 1:10 scaled down model were ten times the velocity used when simulating the full scale geometry.

3.1.1. Pressure and velocity measurement for the benchmark model

Fig. 8 depicts a comparison of the average air velocity values between the wind tunnel measurements and the CFD results of the benchmark model plotted against the back blowing air velocity. The two vertical planes were located upstream and downstream the seated group of spectators, as shown in Fig. 4. Fig. 8 shows a maximum difference of about 5% at back air blowing velocity of 0.7 m/s. Other velocity values comparisons show good agreement between measured and predicted results. Measurements were repeated for 10 times to obtain the mean values. Error bars shown in the figure represent the standard deviation at each location. The maximum standard deviation was found to be about 0.1 m/s.

Fig. 9 shows a comparison between the wind tunnel measured air pressure values and the numerical predicted pressure values for the benchmark model against the back air blowing velocity. The results plotted are for the vertical planes considered previously, upstream and downstream the seated spectators. A maximum difference of 8.6% was recorded at an air velocity of 1.1 m/s at the plane upstream the seated spectators. The comparison shows good agreement between the numerical model and the experimental results. The pressure was measured 10 times at each location to obtain mean values. The error bars shown in Fig. 9 represent the standard deviation at each location. For these measurements, the maximum standard deviation was found to be about 0.05 Pa.

Fig. 10, depicts a comparison between the mean measured values and predicted average air velocity values at 8 equally spaced positions, as shown in Fig. 4, along a line cutting through the seven rows of seated spectators. The measured velocity standard deviations are shown in Table 2. Due to the bluff body shape of the spectators, the flow is characterized by unsteady and fluctuating air velocity values. The unsteady velocity values obtained from simulations were curve fitted with a third degree polynomial curve, and then compared to the average measured velocity values. Average recorded differences between both measured and predicted air velocity values were about 5%.

3.1.2. Standalone model velocity field validation using PIV

Fig. 11 compares the velocity field vectors obtained using PIV with the CFD results past the spectators setting on the bleachers. The vectors shown are colored by velocity magnitude in (m/s). The results are divided into 3 sections that cover the length of the 7 rows of the model, and this is made in order to have a good PIV resolution. PIV results were compared to their numerical counterparts at the same locations. The comparison showed good agreement between both approaches. Qualitatively, the general flow field around the spectators was similar. However, some areas near spectators' legs were not completely captured due to spectators' bodies shadowing the laser beam.

The graph in Fig. 12 shows the variation of the velocity magnitude along a line passing over the heads of the spectators (last set of spectators to the right of Fig. 4) at a height of 1 cm. The figure shows a comparison between simulated velocity values and their PIV measured counterparts at the same location. The error bars in Fig. 12 represent the standard deviation error. The uncertainty form the PIV results is large at the start of the spectator's model and at its end downstream. This is because the laser sheet strength is not uniform. At the sides, tracer particles are less illuminated because the sheet strength is less. For positions 3 to 6, the uncertainty is low as they are located at the middle portion of the laser sheet. The maximum value for the standard deviation of the PIV results was about 0.5 m/s. This deviation is due to the error resulting from uniformity of seeding. The comparison shows good agreement between the average values of velocities obtained by both investigations. The best agreement obtained is at the locations from 3 to 6, and the results yielded an absolute average error of 11%.

3.2. Utilization of porous models

In this subsection, the simulation results for the benchmark model are used to obtain the required coefficients for the two porous media models. The coefficients obtained will be used to perform simulations using each model. Hence, the results of the 3D porous volume and the 2D porous jump models are compared with the cases of empty tiers and detailed spectators. Finally, the coefficients for the porous media models will be used in the standalone model for further validation and comparison with the acquired PIV results.

3.2.1. CFD simulations for identification of the porous models' coefficients (benchmark model)

The results obtained in section 3.1 are used here to obtain the coefficients for the 3D porous volume and the 2D porous jump models. To determine the coefficients C_0 and C_1 for the 3D porous volume model (equation (3)), the case for the detailed spectators' geometry

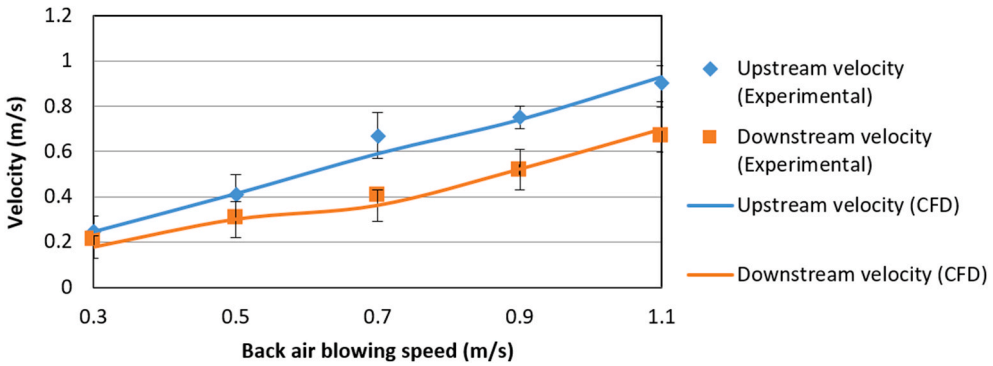

Fig. 8. Comparison of the average air velocity upstream and downstream the seated spectators (locations indicated in Fig. 4).

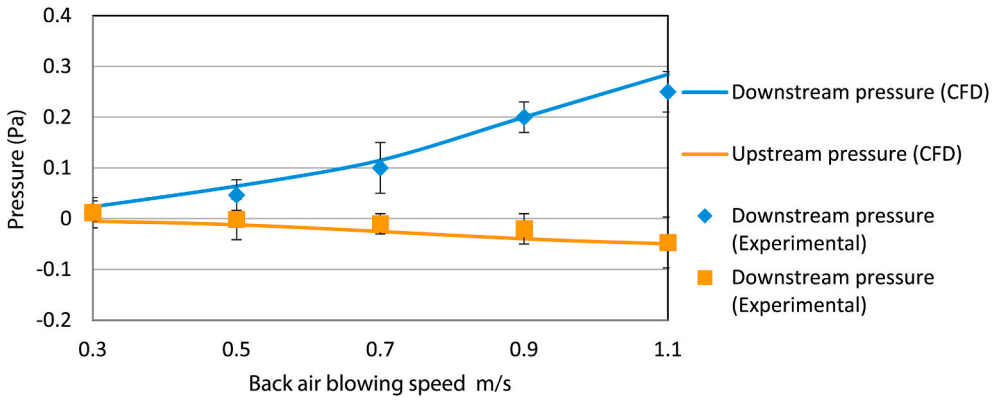

Fig. 9. Comparison of the average air pressure upstream and downstream the seated spectators (locations indicated in Fig. 4).

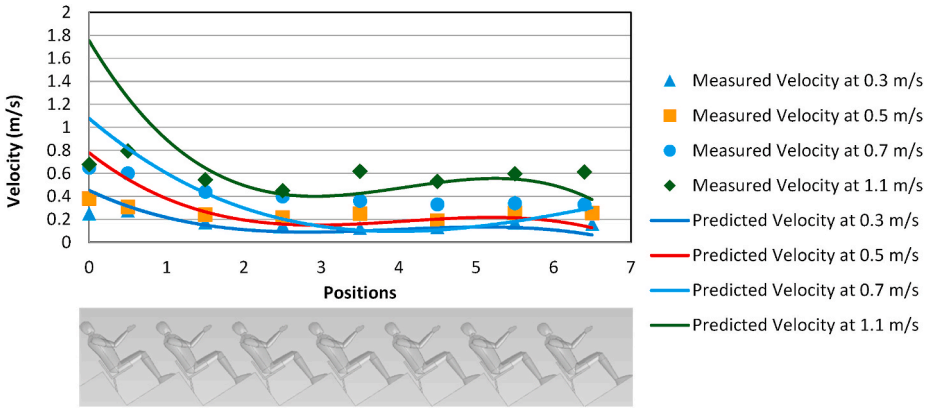

Fig. 10. Comparison of the average air velocity at centerline (location indicated in Fig. 4).

Table 2
Standard deviations of velocity measurement at each location.

Point	Velocity (m/s)				
	0.3	0.5	0.7	0.9	1.1
1	0.01	0.019	0.023	0.029	0.038
2	0.01	0.016	0.016	0.023	0.049
3	0.014	0.02	0.012	0.021	0.033
4	0.01	0.018	0.014	0.031	0.038
5	0.005	0.014	0.011	0.032	0.0543
6	0.007	0.015	0.009	0.02	0.041
7	0.007	0.012	0.021	0.024	0.04

(benchmark model), was run five times for different free stream air velocity values of (1, 3, 5, 7 and 10 m/s). This was performed to obtain a power law relation between the air velocity and the pressure drop through the porous volume representing the 28 spectators. Table 3 describes the pressure drop of the benchmark model measured between two vertical planes upstream and downstream the spectators' area, as indicated in Fig. 4.

Fig. 13 depicts the mathematical relation, using a power law curve fitting equation, between the pressure drop and the air velocity for the benchmark model. The R2 value for the power law interpolation was 0.8979. The results were used to obtain the required 3D porous volume model coefficients (C_0 and C_1).

With regards to the two-dimensional porous jump modeling, rows of spectators were replaced with a surface of zero thickness. Each of these surfaces was described in the boundary conditions as a 2D porous jump of a defined thickness (Δn), an inertial resistance factor (C_2), and a permeability (α). The surface thickness was selected to be equal to 0.4 m representing the width of the spectators' side. Fig. 14 shows a second order polynomial curve fitting for the same data obtained in Table 3. The R2 value for the polynomial interpolation was 0.9992.

Combining equations (2) and (5), and making an analogy with equation (7), the coefficients A and B obtained from the second order polynomial curve fitting in Fig. 14 can be used to estimate the values of C_2 and $1/\alpha$. From the knowledge of $A = 0.3853$ and $B = 0.0483$, and with $\rho = 1.225\ \mathrm{kg/m^3}$, and a porous media thickness $\Delta n = 0.4$ m, the inertial resistance coefficient were calculated as $C_2 = 1.587$ (1/m). Likewise, for the viscous resistance coefficient, with a dynamic viscosity $\mu = 1.7894 \times 10^{-5}\ (\mathrm{m^2/s})$, it can be found out that $\frac{1}{\alpha} = 447\ (1/\mathrm{m^2})$. The values obtained for C_2 and α were used in ANSYS Fluent for the two-dimensional porous jump model simulations.

3.2.2. *Comparison of the performance of different porous models (benchmark model)*

Following the numerical model validation and in order to assess the performance of the porous models, four different cases for the benchmark model were simulated. The air flow was supplied at 3 m/s from overhead mounted jets and delivering conditioned air to the stadium. To observe the aerodynamic effect of the spectators' body, a numerical model of empty tiers was simulated for comparison with the exact geometrical model. Hence, two other cases were simulated using the 3D porous volume and the 2D porous jump model. Using the porous model coefficients obtained in the previous section, numerical simulations using the 3D porous volume and 2D porous jump were performed to capture the aerodynamic effect of the spectators. The results obtained from the two porous models were compared to the results of the other cases.

Fig. 15 depicts the pressure contours along a central vertical plane cutting through the stadium for all the four cases, empty bleachers

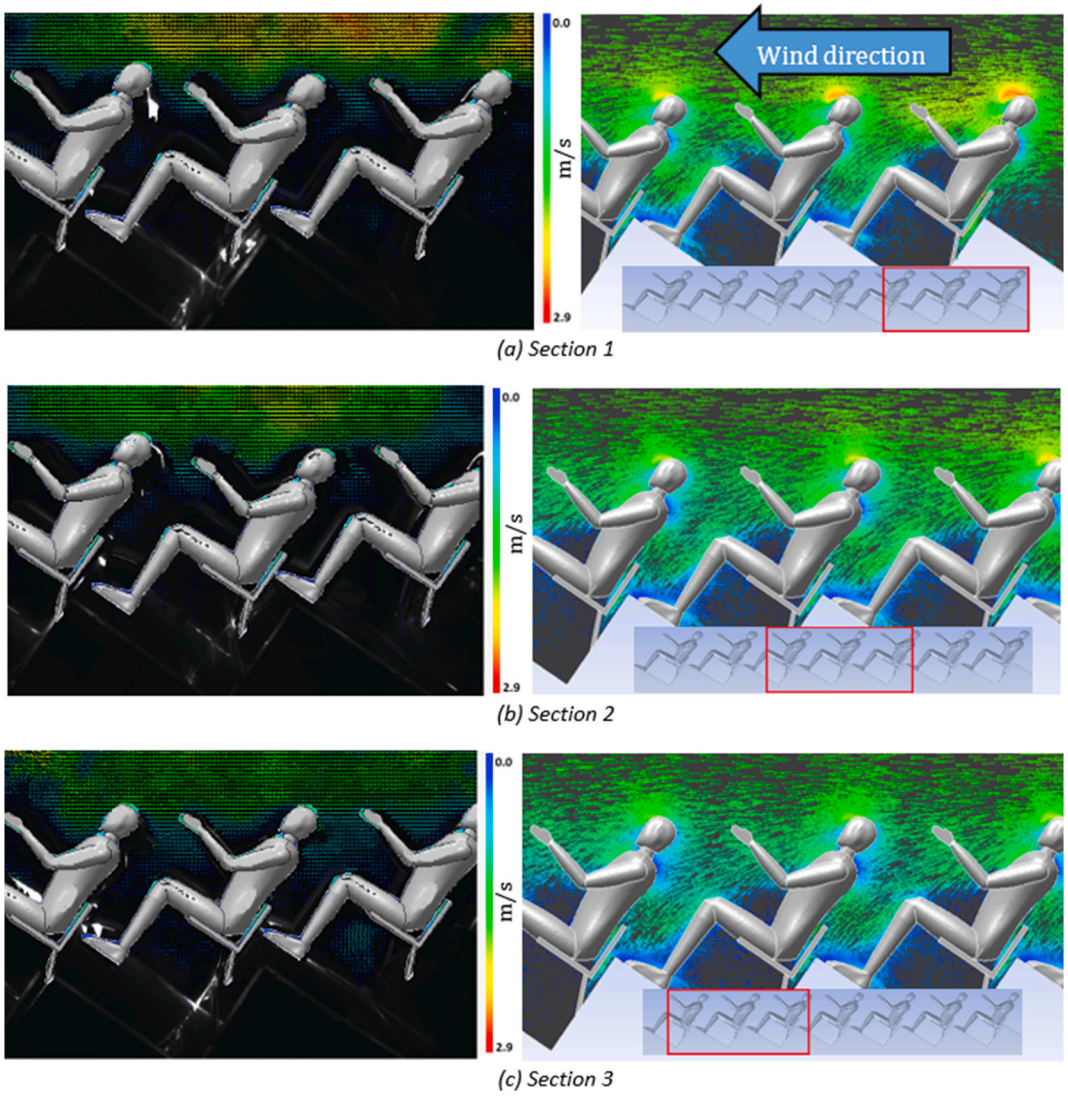

Fig. 11. Velocity vectors past the spectators obtained from PIV (left column) and CFD (right column) colored by their magnitude for sections 1, 2 and 3 (m/s).

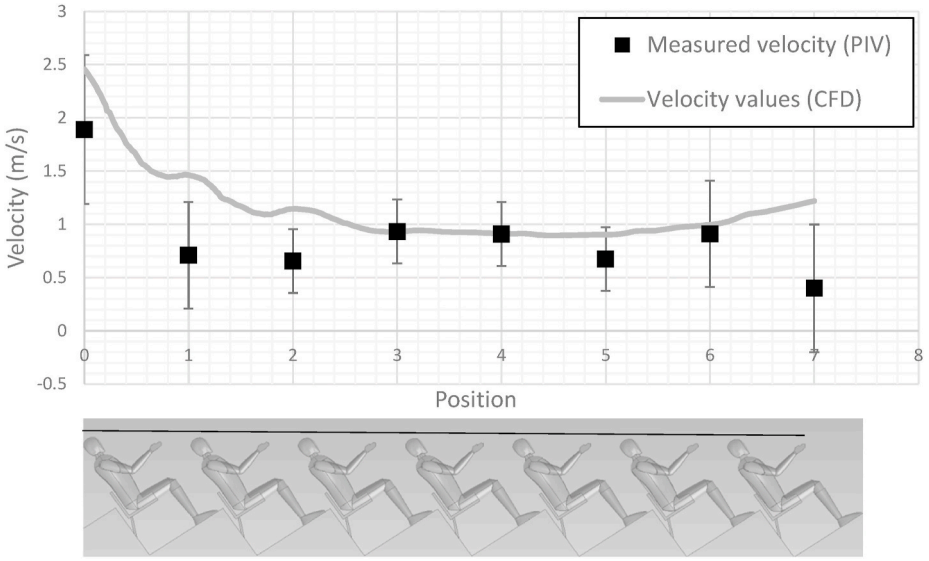

Fig. 12. Velocity magnitude variation along a line passing just above spectators' heads.

Table 3
Pressure drop with inlet velocity (benchmark model).

Velocity (m/s)	P_1 upstream the spectators	P_2 downstream the spectators	ΔP (Pa)
1	1.128	0.18	0.948
3	5	1.15	3.85
5	15	5.75	9.25
7	28.9	9.4	19.5
10	55	16	39

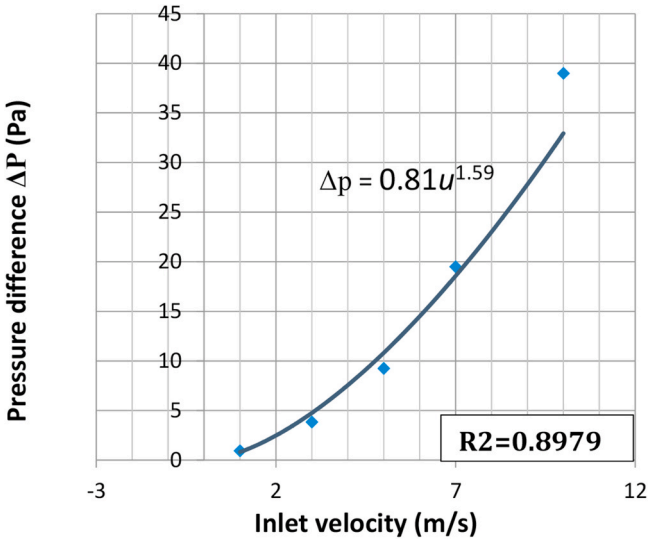

Fig. 13. Pressure difference change with incident air velocity.

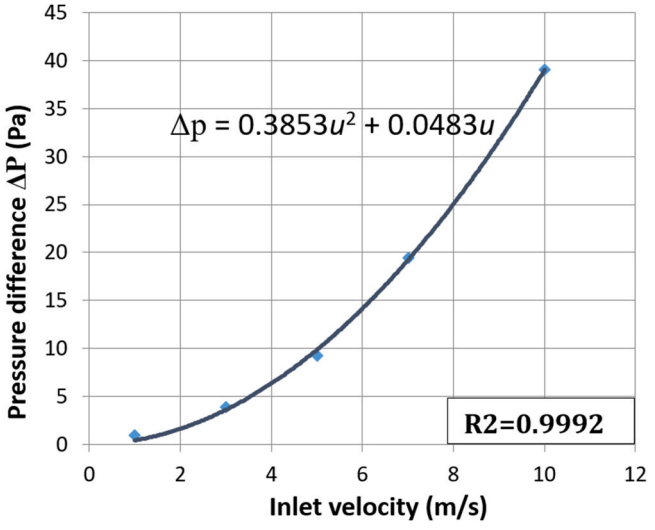

Fig. 14. Pressure difference change with incident air velocity.

(panel (a)), the detailed geometry of the spectators (panel (b), the 3D porous volume (panel (c)), and the 2D porous jump (panel (d)). The pressure drop due to the presence of the spectators (panel (b)) is not captured when simulating empty bleachers (panel (a)). Using a 3D porous volume (panel (c)) results in a pressure drop, however, the wake size is larger than the case with detailed spectators. The 2D porous jump model (panel (d)), was able to produce a pressure drop and a wake size that are in more agreement with the case of detailed spectators (panel (a)).

Fig. 16 shows the velocity contours of the four cases plotted with air blowing at 3 m/s from the overhead jet nozzles. The velocity contours in panel (b) show the effect of spectators' bluff bodies on the air downstream. The air velocity values increased at the spectators' head level and in the vicinity between spectators. Whereas in panel (a), the empty bleachers act as air flow dampers as higher velocity values occur at the tier top and hence reduced as the flow trickles down the empty tiers. Panels (c) and (d) show the velocity contours acquired for the 3D porous volume and the 2D porous jump, at the central vertical plane cutting through the tiers. In both panels, deceleration of the air flow through the tiers is evident with higher air velocities at the top of the tiers. The larger wake area of the 3D porous volume model results is also evident in Fig. 16 panel (c).

Fig. 17 presents a summary of the comparison of the average air velocity profiles along a centerline passing parallel through the 7 rows and positioned at a height of 1 m above the tiers surface for the cases considered. In comparison to the case with detailed 28 spectators, the empty tiers case depicted a higher velocity profile as the spectators present considerable aerodynamic drag to the air flow. An average air velocity difference of about 9.6% occurred about 1 m upstream of the tier length. Hence, this average velocity value difference increased to about 22.4% for the rest of the tiers. This result showed that the effect of spectators drag on air flow cannot be neglected. In comparison to the benchmark model, the 3D porous volume model shows that it can capture the momentum loss due to the presence of the spectators with an average error of 9.1% at the first 1.5 m of the tier, while the average error was increased to 19.8% along the rest of the tier. However, when the model was simulated with 2D porous jump planes replacing each row of seated spectators, the average error in the first 2 m yielded 12.5%, while the average error in the rest of the line (positions 3 to 6) was about 1.5%. The case with empty bleachers and the 3D porous volume model yielded a larger error at the locations 3 to 6, with errors of 27.2% and 24.5% respectively. The processing of the detailed spectators' model configuration took about 36 h to reach converged solution using on a parallel computing hardware with eight cores each of 2.9 GHz, while the 3D porous volume and the 2D porous jump models processing time took about 3 h.

3.2.3. *Validation of porous models with the standalone model*

Fig. 18 shows a comparison of the air velocity profile along a line passing at 1 cm height above the heads of spectators for the standalone model (Fig. 12). The simulations using the values obtained for the porous models' coefficients were validated against the velocities obtained from the PIV. The figure compares the exact geometrical standalone model, empty bleachers case, 3D porous volume, 2D porous jump, and the PIV results. Downstream the spectators (position 7), the results of the exact geometrical model show that due to the presence of spectators, the upstream velocity was decreased by 46% when compared to the case of empty bleachers. The 3D porous volume results have less agreement with results from both obtained by PIV and the simulation of the exact geometry. At position 7, the upstream velocity was decreased by only 27% when using the 3D porous volume model, which is 19% higher than the exact geometry case. The 2D porous jump performed better, as the velocity downstream was decreased by 44.7%.

Table 4 summarizes the root-mean square error (RMSE) obtained when comparing the various models to the PIV and the exact geometry CFD results. The errors shown in Table 4 are computed for the locations 3 to 6, where the flow is not affected by the upstream and downstream conditions. Compared to PIV, the exact geometry and the 2D porous jump, had similar RMSE values of 0.27 and 0.37 m/s respectively. Compared to the exact geometry, the 2D porous jump had an RMSW error of 0.25 m/s, while the 3D porous volume yielded a larger error of 0.55 m/s.

3.3. *Effect of velocity field on thermal comfort prediction*

To illustrate the effect of the predicted velocity fields on the SET and

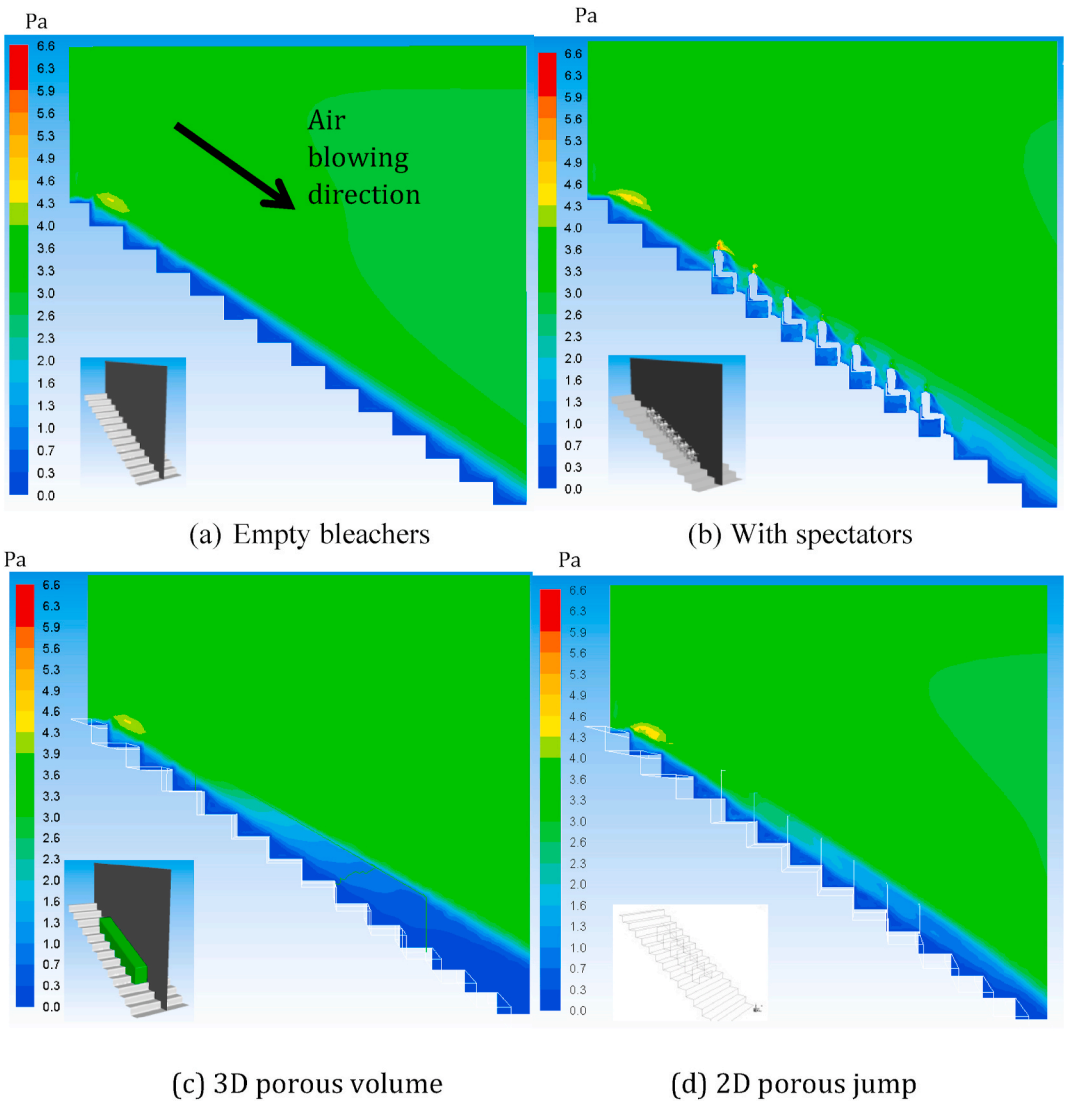

Fig. 15. Pressure contours at 3 m/s blowing back air for four different cases (benchmark model).

UTCI values, four cases with identical boundary conditions were compared. To evaluate the thermal comfort and calculate the cooling load, both the energy equation and the species transport model need to be considered. The boundary conditions were defined such that the far field has a temperature of 30°C and relative humidity 60% which corresponds to the average weather conditions in the hot and arid areas [22]. The conditioned air is released from the back of the spectators with an inlet velocity of 0.5 m/s, a temperature of 17°C, and a relative humidity of 80%. The cases considered were: empty bleachers, with spectators, 3D porous volume and 2D porous jump. This comparison will also aid in the assessment of the performance of the different porous models. The results shown here are for the standalone model (previously illustrated in Fig. 7).

The SET is a function of various factors as follows [60]:

$$\mathrm{SET} = f(u, T_{air}, p, RH, clo, met) \tag{11}$$

where u is the air velocity (m/s), T_{air} is the ambient air temperature (°C), p is the pressure (Pa), RH is the relative humidity (%), clo is the clothing factor, and met is the metabolic rate of the individual. The clothing factor was set to 0.62 and the metabolic rate was set to 1.2, to represent seated spectators wearing summer clothing. The evaluation of the UTCI is performed using a 6th order degree polynomial approximation [64].

Fig. 19 shows the contours for the SET for the different cases. The values shown are plotted at a plane placed in a height such that it is passing through the spectators' shoulders. The cases without and with spectators are shown in panels (a) and (b). Whereas the lower panels (c) and (d), show the SET obtained using the 3D porous volume and 2D porous jump respectively. In the case of empty bleachers, panel (a), the cold air does not travel further downstream compared to the case with spectators (panel (b)). Moreover, in the case with spectators, the values inside the spectator's area were higher and more confined, differently from the case with empty bleachers. Moving on to panels (c) and (d), in both cases the cold air travels downstream to a distance further than the empty bleachers case. However, the SET distribution is captured more accurately when using the 2D porous jump model (panel (d)), than using the 3D porous volume model (panel (c)).

Fig. 20 shows the contours of UTCI for the cases considered. Similarly to the SET in Fig. 19, in the case of empty bleachers (panel (a)) the region of low UTCI values is confined to the bleachers area, and does not move further downstream. The 3D porous volume (panel (c)) and the2D porous jump models (panel (d)) both show similar contours of UTCI, that are in better agreement with the case of detailed spectators in panel (b).

Table 5 compares the average SET, UTCI, and the total cooling load for the four different cases plotted in Figs. 19 and 20. Two average SET and UTCI values were obtained for the whole plane. The cooling load is calculated for the whole bleachers area, and not just the spectators.

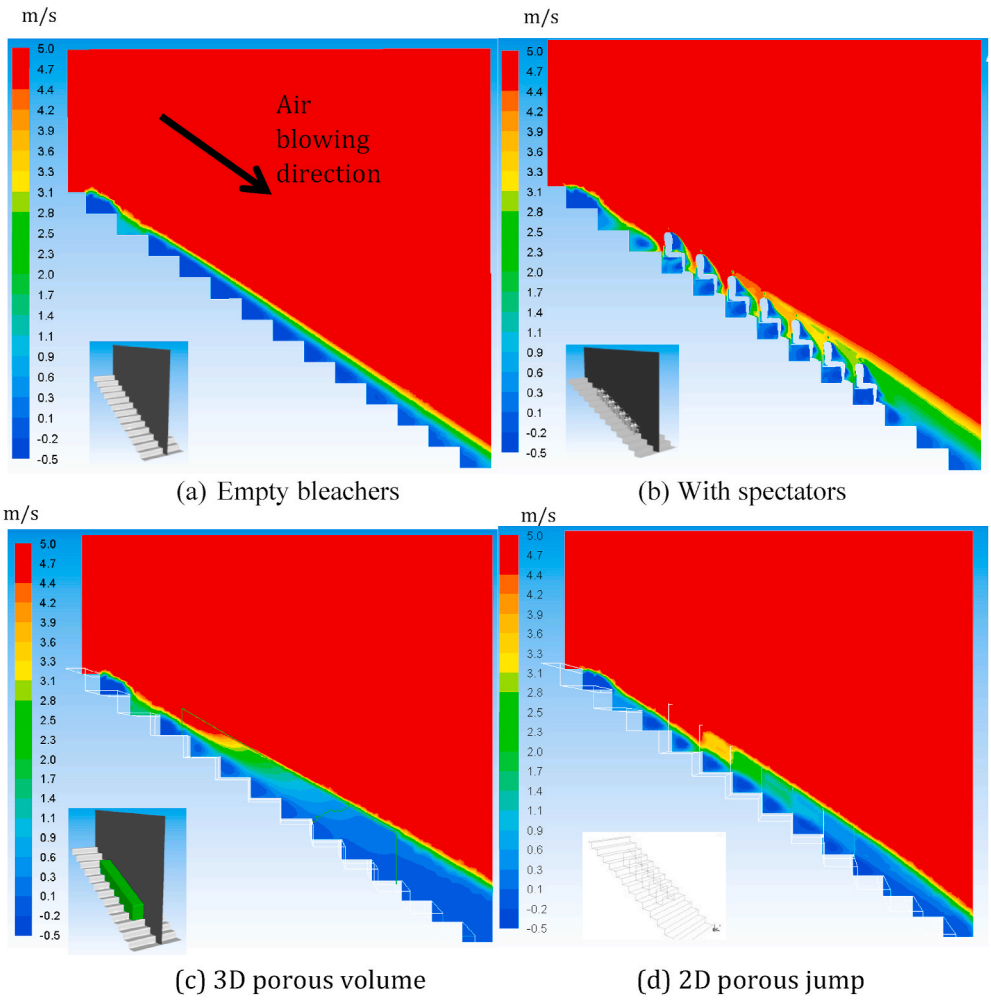

Fig. 16. Velocity contours at 3 m/s blowing back air for four different cases (benchmark model).

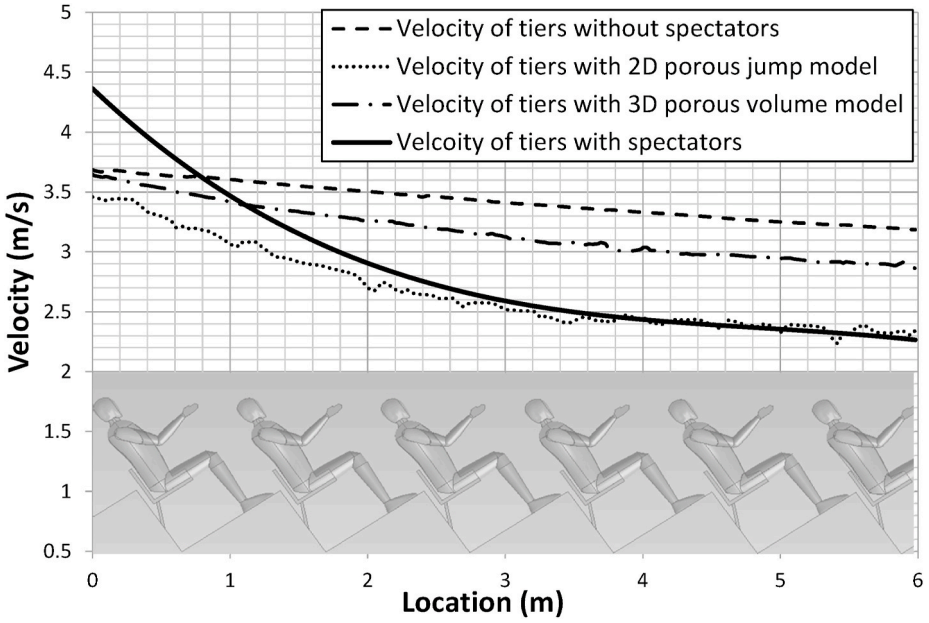

Fig. 17. Air velocity profile along an inclined line passing through the rows for the benchmark model.

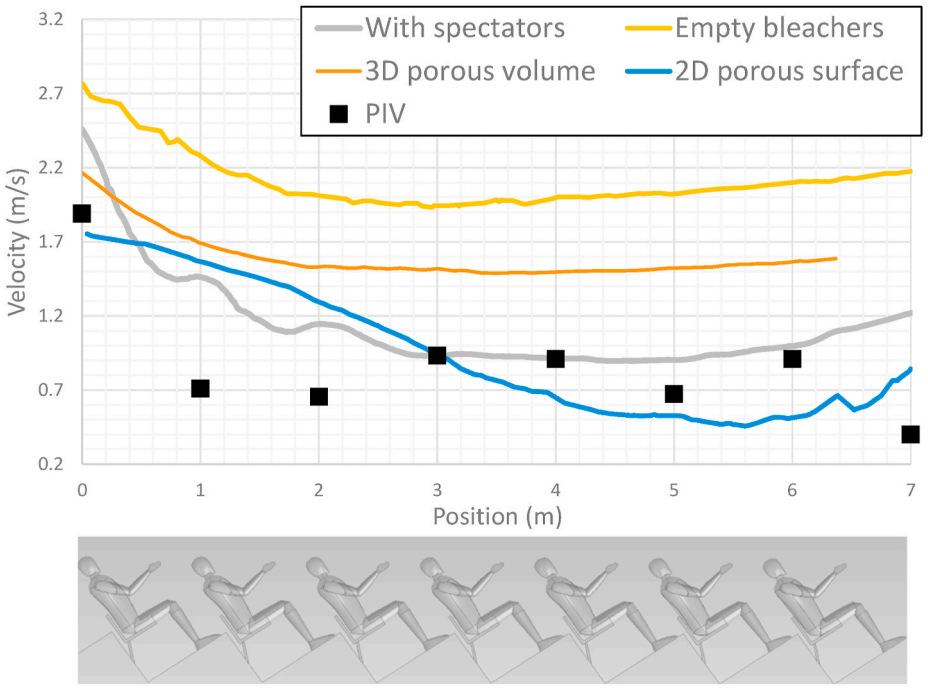

Fig. 18. Comparison of the results obtained for the standalone model.

Table 4
RMSE error for the standalone model.

Error when comparing with:	Exact geometry	3D porous volume	2D porous jump
RMSE (m/s) (PIV)	0.27	0.73	0.37
RMSE (m/s) (CFD of exact geometry)	N/A	0.55	0.25

The average SET yielded the largest value of 21°C for the case of empty bleachers. This is because the cold air did not travel further downstream, and hot regions cover a larger portion of the plane. The case with spectators yielded an average SET value of 20.32°C, and the model closest to it was the 2D porous jump with an average SET of 20.22°C. With regard to the average UTCI values, the case with spectators yielded an average UTCI of 21.7°C, and the case of empty bleachers overestimated this value by 2°C. Both porous models overestimated the average UTCI value, but the 2D porous jump model was the closest to the case with spectators, with an average UTCI of 23.1°C.

The calculation for the total cooling load was performed using equations (8)–(10), and the values used are the average quantities at the plane for each case. The calculations were performed on rows 3 to 6 because in these rows the effect of the spectator's body is dominant and it is far from the inlet and exit boundaries. The cooling load for the 2D porous jump was closest to the case with spectators with an absolute relative error of 6%. The 3D porous volume performed worse than the 2D porous jump model and yielded an error of 6.5%. However, both porous models performed better than the case with empty bleachers where the cooling load was under-estimated by 16.9%.

4. Conclusion

This paper assessed the utilization of porous models to simulate the drag effect of spectators in large air-conditioned buildings such as stadiums. The use of 2D and 3D porous media models to represent the aerodynamic effect of the spectators on the flow field inside a stadium was assessed. Comparison of predicted average air velocity between empty stadium section model and the benchmark stadium section model with 28 spectators showed a difference of 27.2%. Using the 3D porous volume model to replicate the aerodynamic effect of detailed spectators' geometry managed to reduce the required processing time. However, this approximation resulted in an average error of 24.5% compared to the benchmark model with detailed geometrical features. Using a 2D porous jump model of a width of 0.4 m to replicate the aerodynamic effect of detailed spectators' geometry yielded an average error of 1.5% compared to the benchmark model with detailed geometrical features. Utilization of the porous models reduced the model grid size from about 12,000,000 to only 900,000 elements yielding acceptable accuracy. Using a parallel computing hardware with eight cores each of 2.9 GHz, the associated processing time required for convergence of the porous models was reduced by 90% in comparison to the benchmark model of detailed microscopic section.

For validation, the results of a standalone model were compared to PIV results. The results confirmed that the 2D porous jump model performed better than the 3D porous volume model. Compared to PIV, the 2D porous jump had an RMSE value of 0.37 m/s, and the 3D porous volume yielded an RMSE of 0.73 m/s. The comparison with the exact geometry CFD results yielded an RMSE of 0.25 m/s for the 2D porous jump, and 0.55 m/s for the 3D porous volume.

The usage of porous models affected the values of the evaluated thermal comfort indices. In a plane passing through the spectators' shoulders, the average SET was 20.32°C for the case with spectators and 21°C for the case of empty bleachers. This error will propagate to the prediction of HVAC systems' performance and cooling load calculations. Using the porous media model yielded an average SET of 20.17°C and 20.22°C for the 3D porous volume and 2D porous jump models respectively. The 2D porous jump model had a less agreement for the average UTCI value, however it performed better than the 3D porous volume model. For the total cooling load, the 2D porous jump model performed best with an error of 6%, compared to an error of 6.5% for the 3D porous volume model.

The results showed that in all cases, the usage of porous models provide results that are in better agreement with the actual case than simulating empty bleachers. In terms of velocity field and thermal comfort evaluation, the 2D porous jump model was superior to the 3D porous volume model. In conclusion, the 2D porous jump model

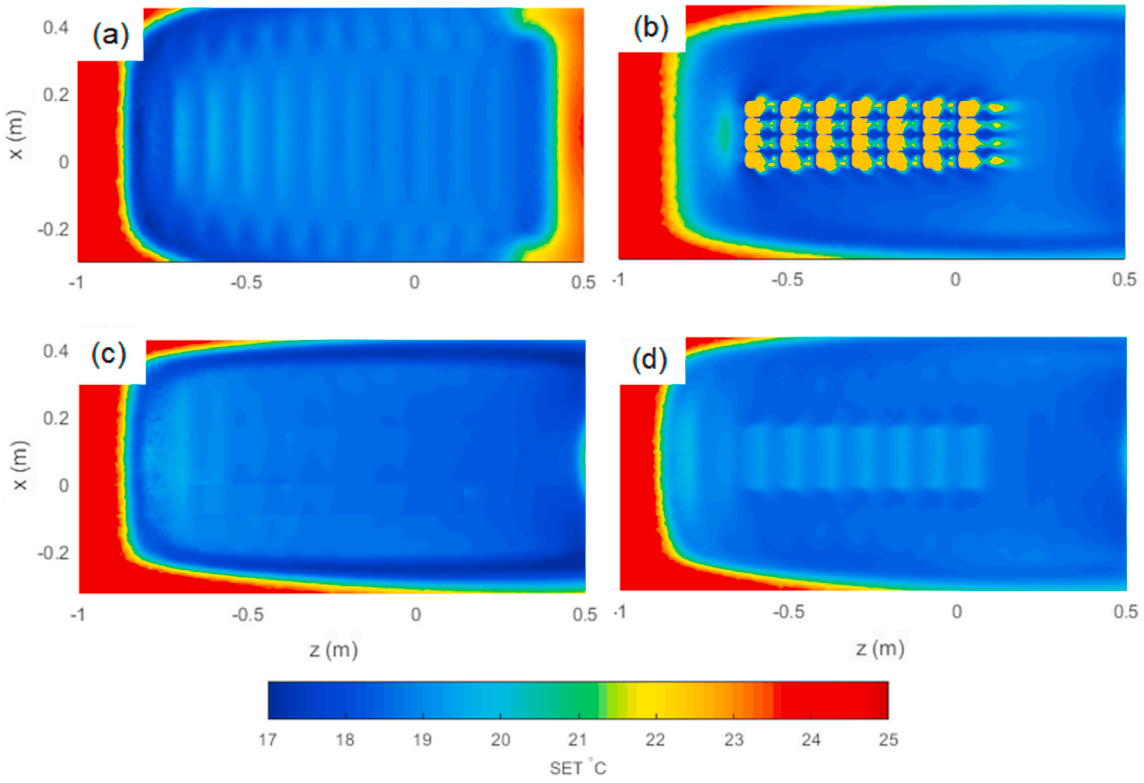

Fig. 19. Comparison of CFD predicted SET values for simulation of the stadium tiers (a) without spectators, (b) with spectators, (c) using 3D porous volume and (d) using 2D porous jump.

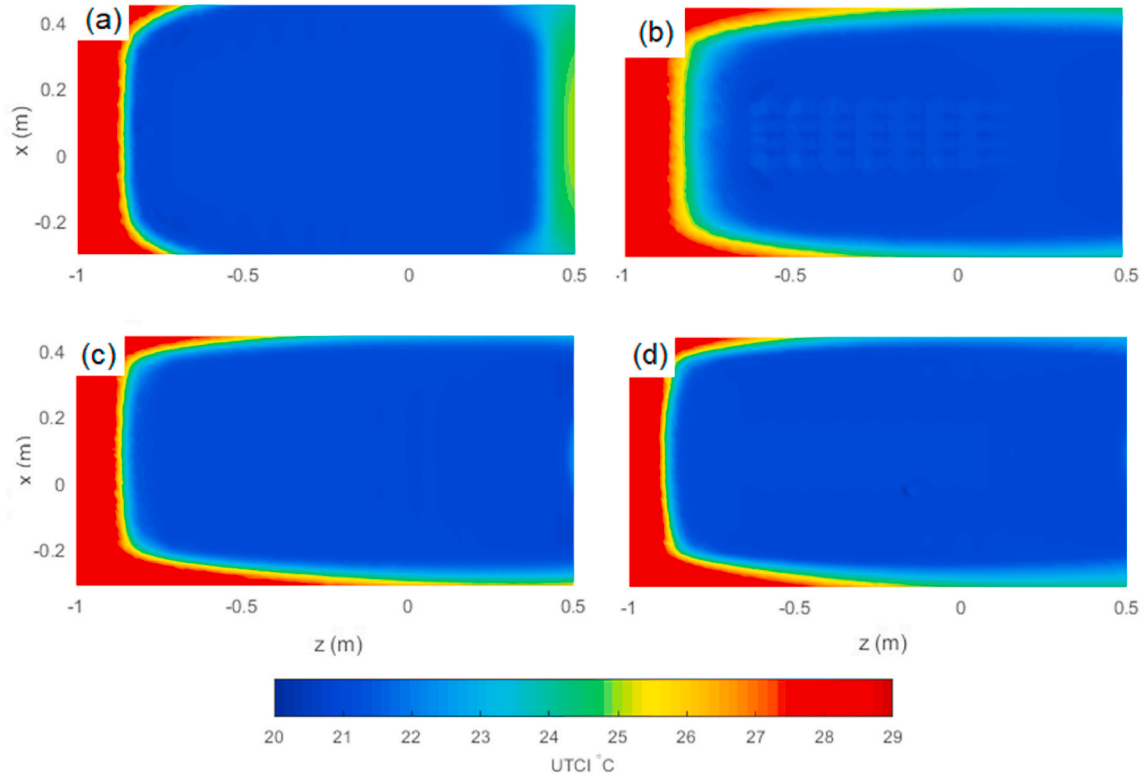

Fig. 20. Comparison of CFD predicted UTCI values for simulation of the stadium tiers (a) without spectators, (b) with spectators, (c) using 3D porous volume and (d) using 2D porous jump.

Table 5
Average SET values obtained from different models.

Model	Average SET (°C)	Average UTCI (°C)	Cooling load (kW) (Bleachers region)
Without spectators	21	23.7	6.84
With spectators	20.32	21.7	8.23
3D porous volume	20.2	23.2	7.69
2D porous jump	20.22	23.1	7.73

provided a better option to represent spectators within the stadium. Utilization of the 2D porous jump managed to simulate the spectators' drag effect on supplied air. This method provides significant savings of the processing time and reduces the required computational hardware and the associated costs with an acceptable aerodynamic accuracy.

In future work, porous models can be assessed to represent large crowds inside other indoor and outdoor environments such as theatres.

Declaration of competing interest

The authors declare that they have no known competing financial interests or personal relationships that could have appeared to influence the work reported in this paper.

Acknowledgments

The work presented in this paper was supported by the Aspire Zone Foundation [External grant number QUEX-CENG-ASPIRE-11/12-7] and by a grant from the Qatar National Research Fund under its National Priorities Research Program [Award number NPRP 6-461-2-188]. The statements made herein are solely the responsibility of the authors.

References

[1] A. Banerjee, S. Pasupuleti, G.N. Pradeep Kumar, S.C. Dutta, A three-dimensional CFD simulation for the nonlinear parallel flow phenomena through coarse granular porous media, Appl. Fluid Dyn. (2018) 469–480, https://doi.org/10.1007/978-981-10-5329-0_34.
[2] H. Liu, Q. Kang, C.R. Leonardi, S. Schmieschek, A. Narváez, B.D. Jones, J. R. Williams, A.J. Valocchi, J. Harting, Multiphase lattice Boltzmann simulations for porous media applications A review, Comput. Geosci. 20 (2016) 777–805, https://doi.org/10.1007/s10596-015-9542-3.
[3] S. Ghani, E.M. Bialy, F. Bakochristou, S.M.A. Gamaledin, M.M. Rashwan, B. Hughes, Thermal comfort investigation of an outdoor air-conditioned area in a hot and arid environment, Sci. Technol. Built Environ. 23 (2017) 1113–1131, https://doi.org/10.1080/23744731.2016.1267490.
[4] G. Ye, C. Yang, Y. Chen, Y. Li, A new approach for measuring predicted mean vote (PMV) and standard effective temperature (SET*), Build. Environ. 38 (2003) 33–44, https://doi.org/10.1016/S0360-1323(02)00027-6.
[5] L. Gu, H. Qi, F. Wu, H. Liu, CFD numerical simulation of typical shape stadiums, Spat. Struct. 2 (2010).
[6] T. Van Hoof, B. Blocken, Computational analysis of natural ventilation in a large semi-enclosed stadium, in: EACWE 5, 2009 (Florence, Italy).
[7] T. van Hooff, B. Blocken, CFD analysis of natural ventilation in large semi-enclosed buildings – case study: Amsterdam Arena football stadium, Elev. Int. IBPSA Conf. Glas. Schotl. (2009) 27–30.
[8] D. Delaunay, L. Di, S. Bodere, Calibrating a CFD canopy model with the EC1 vertical profiles of mean wind speed and turbulence, in: 13 International Conference on Wind Engineering, 2011 (Amsterdam).
[9] A. Gosman, Developments in CFD for industrial and environmental applications in wind engineering, J. Wind Eng. Ind. Aerod. 81 (1999) 21–39, https://doi.org/10.1016/S0167-6105(99)00007-0.
[10] T. van Hooff, B. Blocken, Coupled urban wind flow and indoor natural ventilation modelling on a high-resolution grid: a case study for the Amsterdam ArenA stadium, Environ. Model. Software 25 (2010) 51–65, https://doi.org/10.1016/J.ENVSOFT.2009.07.008.
[11] T. van Hooff, B. Blocken, On the effect of wind direction and urban surroundings on natural ventilation of a large semi-enclosed stadium, Comput. Fluids 39 (2010) 1146–1155, https://doi.org/10.1016/j.compfluid.2010.02.004.
[12] L. Chen, Y. Li, Effects of different auditorium forms on ventilation in a football stadium, Indoor Built Environ. 1420326X1987313 (2019), https://doi.org/10.1177/1420326x19873132.
[13] B. Blocken, J. Persoon, Pedestrian wind comfort around a large football stadium in an urban environment: CFD simulation, validation and application of the new Dutch wind nuisance standard, J. Wind Eng. Ind. Aerod. 97 (2009) 255–270, https://doi.org/10.1016/J.JWEIA.2009.06.007.
[14] T. van Hooff, B. Blocken, M. van Harten, 3D CFD simulations of wind flow and wind-driven rain shelter in sports stadia: influence of stadium geometry, Build. Environ. 46 (2011) 22–37, https://doi.org/10.1016/j.buildenv.2010.06.013.
[15] T. van Hooff, M. van Harten, B. Blocken, Numerical analysis of wind-driven rain shelter in sports stadia for different stadium geometries, in: The Fifth International Symposium on Computational Wind Engineering (CWE2010), Chapel Hill, North Carolina, USA, 2010.
[16] J. Persoon, T. van Hooff, B. Blocken, J. Carmeliet, M.H. de Wit, On the impact of roof geometry on rain shelter in football stadia, J. Wind Eng. Ind. Aerod. 96 (2008) 1274–1293, https://doi.org/10.1016/j.jweia.2008.02.036.
[17] T. Uchida, R. Araya, Practical applications of the large-eddy simulation technique for wind environment assessment around new national stadium, Japan (Tokyo olympic stadium), Open J. Fluid Dynam. 9 (2019) 269–291, https://doi.org/10.4236/ojfd.2019.94018.
[18] H.U. Kim, S. Il Jong, Development of a system for evaluating the flow field around a massive stadium: combining a microclimate model and a CFD model, Build. Environ. 172 (2020), https://doi.org/10.1016/j.buildenv.2020.106736, 106736.
[19] X. Zheng, H. Montazeri, B. Blocken, CFD simulations of wind flow and mean surface pressure for buildings with balconies: comparison of RANS and LES, Build. Environ. 173 (2020), https://doi.org/10.1016/j.buildenv.2020.106747, 106747.
[20] S. Murakami, J. Zeng, T. Hayashi, CFD analysis of wind environment around a human body, J. Wind Eng. Ind. Aerod. 83 (1999) 393–408, https://doi.org/10.1016/S0167-6105(99)00088-4.
[21] A.O. Mahgoub, S. Gowid, S. Ghani, Global evaluation of WBGT and SET indices for outdoor environments using thermal imaging and artificial neural networks, Sustain. Cities Soc. 60 (2020), https://doi.org/10.1016/j.scs.2020.102182, 102182.
[22] S. Ghani, E.A. ElBialy, F. Bakochristou, S.M.A. Gamaledin, M.M. Rashwan, B. Hughes, Thermal performance of stadium's Field of Play in hot climates, Energy Build. 139 (2017) 702–718, https://doi.org/10.1016/j.enbuild.2017.01.059.
[23] T. Honjo, Thermal comfort in outdoor environment, Glob. Environ. Res. ©2009 AIRIES 13 (2009) 43–47.
[24] T. Catalina, J. Virgone, F. Kuznik, Evaluation of thermal comfort using combined CFD and experimentation study in a test room equipped with a cooling ceiling, Build. Environ. 44 (2009) 1740–1750, https://doi.org/10.1016/J.BUILDENV.2008.11.015.
[25] H. Awbi, Predicting air flow and thermal comfort in offices, ASHRAE Journal-American Soc. Heat. Refrig. Airconditioning Eng. 36 (1994) 17–23.
[26] Z. Lin, T.T. Chow, K.F. Fong, Q. Wang, Y. Li, Comparison of performances of displacement and mixing ventilations. Part I: thermal comfort, Int. J. Refrig. 28 (2005) 276–287, https://doi.org/10.1016/J.IJREFRIG.2004.04.005.
[27] K.W.D. Cheong, E. Djunaedy, Y.L. Chua, K.W. Tham, S.C. Sekhar, N.H. Wong, M. B. Ullah, Thermal comfort study of an air-conditioned lecture theatre in the tropics, Build. Environ. 38 (2003) 63–73, https://doi.org/10.1016/S0360-1323(02)00020-3.
[28] A.I. Stamou, I. Katsiris, M. Politis, A. Schaelin, Applying A CFD model to evaluate thermal comfort in the MPC Amphitheatre of the olympic games "Athens 2004, Eng. Appl. Comput. Fluid Mech. 2 (2008) 41–50, https://doi.org/10.1080/19942060.2008.11015210.
[29] A.I. Stamou, I. Katsiris, A. Schaelin, Evaluation of thermal comfort in galatsi Arena of the olympics "Athens 2004" using a CFD model, Appl. Therm. Eng. 28 (2008) 1206–1215, https://doi.org/10.1016/j.applthermaleng.2007.07.020.
[30] A.I. Stamou, I. Katsiris, A. Schaelin, Evaluation of thermal comfort in indoor stadiums of the Athens 2004 olympic games with CFD models: case of nikea indoor stadium, J. Architect. Eng. 13 (2007) 130–135, https://doi.org/10.1061/(ASCE)1076-0431(2007)13:3(130).
[31] S.M. Mcguffie, D.H. Martens, M.A. Porter, The Use of Porous Media Models and CFD for Sulfur Treating Applications, 2013 (Lawrence, Kansas).
[32] L. Rong, D. Liu, E.F. Pedersen, G. Zhang, The effect of wind speed and direction and surrounding maize on hybrid ventilation in a dairy cow building in Denmark, Energy Build. 86 (2015) 25–34, https://doi.org/10.1016/J.ENBUILD.2014.10.016.
[33] S. Ghani, E.M.A.A. El-Bialy, F. Bakochristou, M. Mohamed Rashwan, A. Mohamed Abdelhalim, S. Mohammad Ismail, P. Ben, Experimental and numerical investigation of the thermal performance of evaporative cooled greenhouses in hot and arid climates, Sci. Technol. Built Environ. 26 (2020) 141–160, https://doi.org/10.1080/23744731.2019.1634421.
[34] J. Roy, T. Boulard, CFD prediction of the natural ventilation in a tunnel-type greenhouse: influence of wind direction and sensibility to turbulence models, in: International Conference on Sustainable Greenhouse Systems-Greensys2004, vol. 691, 2004, pp. 457–464.
[35] A.A. Sapounas, C. Nikita-Martzopoulou, G. Martzopoulos, Numerical and experimental study OF fan and pad evaporative cooling system IN a greenhouse with tomato crop, Acta Hortic. (2008) 987–994, https://doi.org/10.17660/ActaHortic.2008.801.117.
[36] S. Saneinejad, P. Moonen, J. Carmeliet, Coupled CFD, radiation and porous media model for evaluating the micro-climate in an urban environment, J. Wind Eng. Ind. Aerod. 128 (2014) 1–11, https://doi.org/10.1016/j.jweia.2014.02.005.
[37] C. Ooi, P.H. Chiu, V. Raghavan, S. Wan, H.J. Poh, Porous media representation of louvers in building simulations for natural ventilation, J. Build. Perform. Simul. 12 (2019) 494–503, https://doi.org/10.1080/19401493.2018.1510544.
[38] S. Abishek, A.J.C. King, R. Mead-Hunter, V. Golkarfard, W. Heikamp, B.J. Mullins, Generation and validation of virtual nonwoven, foam and knitted filter (separator/

coalescer) geometries for CFD simulations, Separ. Purif. Technol. 188 (2017) 493–507, https://doi.org/10.1016/J.SEPPUR.2017.07.052.
[39] A. d'Hueppe, M. Chandesris, D. Jamet, B. Goyeau, Boundary conditions at a fluid–porous interface for a convective heat transfer problem: analysis of the jump relations, Int. J. Heat Mass Tran. 54 (2011) 3683–3693, https://doi.org/10.1016/J.IJHEATMASSTRANSFER.2011.01.033.
[40] Z. Feng, Z. Long, Q. Chen, Assessment of various CFD models for predicting airflow and pressure drop through pleated filter system, Build. Environ. 75 (2014) 132–141, https://doi.org/10.1016/J.BUILDENV.2014.01.022.
[41] S. Lal, F. Lucci, T. Defraeye, L.D. Poulikakos, M.N. Partl, D. Derome, J. Carmeliet, CFD modeling of convective scalar transport in a macroporous material for drying applications, Int. J. Therm. Sci. 123 (2018) 86–98, https://doi.org/10.1016/J.IJTHERMALSCI.2017.09.010.
[42] A. Della Torre, G. Montenegro, A. Onorati, G. Tabor, CFD characterization of pressure drop and heat transfer inside porous substrates, Energy Procedia 81 (2015) 836–845, https://doi.org/10.1016/J.EGYPRO.2015.12.093.
[43] C. Yue, Q. Zhang, Z. Zhai, Numerical simulation of the filtration process in fibrous filters using CFD-DEM method, J. Aerosol Sci. 101 (2016) 174–187, https://doi.org/10.1016/J.JAEROSCI.2016.08.004.
[44] L. Guo, R.G. Maghirang, Numerical simulation of airflow and particle collection by vegetative barriers, Eng. Appl. Comput. Fluid Mech. 6 (2012) 110–122, https://doi.org/10.1080/19942060.2012.11015407.
[45] P.W. Bearman, Vortex shedding from oscillating bluff bodies, Annu. Rev. Fluid Mech. 16 (1984) 195–222, https://doi.org/10.1146/annurev.fl.16.010184.001211.
[46] D. Thevenin, G. Janiga, Optimization and Computational Fluid Dynamics, Springer, 2008, https://doi.org/10.1007/978-3-540-72153-6.
[47] A. Roshko, On the drag and shedding frequency of two -dimensional bluff bodies, National Advisory Committee for Aeronautics (NACA) Technical Note 3169 (1954).
[48] FIFA, Football Stadiums Technical Recommendations and Requirements, fifth ed., 2011.
[49] A. Aroussi, S.A.A. Abdul Ghani, E. Rice, PIV measurement and numerical simulation of airflow field in a road vehicle HVAC cowl box, in: SAE Technical Papers, SAE International, 2001, https://doi.org/10.4271/2001-01-0294.
[50] T. Cameron, A.L. Yarin, J.F. Foss (Eds.), Springer Handbook of Experimental Fluid Mechanics, Springer Handbook of Experimental Fluid Mechanics, Springer Berlin Heidelberg, 2007, https://doi.org/10.1007/978-3-540-30299-5.
[51] Dantec Dynamics, DynamicStudio User's Guide, Dantec Dynamics, Skovlunde, Denmark, 2012.
[52] ANSYS Inc, ANSYS Fluent User' S Guide Release 15.0, ANSYS, Inc., Canonsburg, Pennsylvania, 2013.
[53] B.E. Launder, D.B. Spalding, The numerical computation of turbulent flows, Comput. Methods Appl. Mech. Eng. 3 (1974) 269–289, https://doi.org/10.1016/0045-7825(74)90029-2.
[54] P.J. Jones, G.E. Whittle, Computational fluid dynamics for building air flow prediction—current status and capabilities, Build. Environ. 27 (1992) 321–338, https://doi.org/10.1016/0360-1323(92)90033-L.
[55] P.F. Linden, The fluid mechanics of natural ventilation, Annu. Rev. Fluid Mech. 31 (1999) 201–238, https://doi.org/10.1146/annurev.fluid.31.1.201.
[56] U. Drori, V. Dubovsky, G. Ziskind, Experimental verification of induced ventilation, J. Environ. Eng. 131 (2005) 820–826, https://doi.org/10.1061/(ASCE)0733-9372(2005)131:5(820).
[57] U. Drori, G. Ziskind, Induced ventilation of a one-story real-size building, Energy Build. 36 (2004) 881–890, https://doi.org/10.1016/j.enbuild.2004.02.006.
[58] G. Ziskind, V. Dubovsky, R. Letan, Ventilation by natural convection of a one-story building, Energy Build. 34 (2002) 91–101, https://doi.org/10.1016/S0378-7788(01)00080-9.
[59] B. Blocken, Computational Fluid Dynamics for urban physics: importance, scales, possibilities, limitations and ten tips and tricks towards accurate and reliable simulations, Build. Environ. 91 (2015) 219–245, https://doi.org/10.1016/j.buildenv.2015.02.015.
[60] ANSI/ASHRAE, ANSI/ASHRAE Standard 55-2017 : Thermal Environmental Conditions for Human Occupancy, ASHRAE Inc (2017), https://doi.org/10.2172/1025697.
[61] K. Blazejczyk, Y. Epstein, G. Jendritzky, H. Staiger, B. Tinz, Comparison of UTCI to selected thermal indices, Int. J. Biometeorol. 56 (2012) 515–535, https://doi.org/10.1007/s00484-011-0453-2.
[62] G. Jendritzky, R. de Dear, G. Havenith, UTCI-Why another thermal index? Int. J. Biometeorol. 56 (2012) 421–428, https://doi.org/10.1007/s00484-011-0513-7.
[63] A. Matzarakis, F. Rutz, Application of the RayMan model in urban environments, in: Ninth Symposium on the Urban Environment, Meteorological Institute, University of Freiburg, 2010.
[64] P. Bröde, D. Fiala, K. Blazejczyk, Calculating UTCI Equivalent Temperature, 2009, pp. 1–5. … XIII, Univ. ….